CHEMISTRY OF MATERIALS
Article

Chem. Mater. **2011,** *23,* 137–144 137
DOI:10.1021/cm101957k

Nucleation Control in the Aggregative Growth of Bismuth Nanocrystals

Vernal N. Richards, Shawn P. Shields, and William E. Buhro*

Department of Chemistry and Center for Materials Innovation, Washington University, St. Louis, Missouri 63130-4899, United States

Received July 14, 2010. Revised Manuscript Received December 10, 2010

The kinetics and mechanism of Bi-nanocrystal growth from the precursor $Bi[N(SiMe_3)_2]_3$ are determined at various $Na[N(SiMe_3)_2]$ additive concentrations. The results establish that aggregative nucleation and growth processes dominate Bi-nanocrystal formation. The time dependence of the aggregative nucleation rate—the nucleation function—is determined over the range of $Na[N(SiMe_3)_2]$ concentrations studied. The time width of aggregative nucleation (Δt_n) is shown to remain reasonably narrow, and to correlate with the final Bi-nanocrystal size distribution. The maximum aggregative nucleation rate (Γ_{max}) is shown to vary systematically with $Na[N(SiMe_3)_2]$ concentration, producing a systematic variation in the final nanocrystal mean size. The $Na[N(SiMe_3)_2]$ additive functions as both a nucleation-control agent and an Ostwald-ripening agent.

Introduction

We show here that aggregative nucleation and growth contribute extensively to the formation of Bi nanocrystals from the precursor $Bi[N(SiMe_3)_2]_3$.[1−5] The characteristics of the aggregative-nucleation process determine the size and size distribution of the Bi nanocrystals at the end of the aggregative-growth regime. Added $Na[N(SiMe_3)_2]$ is shown to function as both a nucleation-control and Ostwald-ripening agent.

Bi nanoparticles are used to catalyze the growth of semiconductor nanowires[2,4,6−23] by the solution−liquid−solid (SLS) mechanism.[24,25] We reported a synthesis of such Bi catalyst nanoparticles that uses $Bi[N(SiMe_3)_2]_3$ as the Bi precursor and $Na[N(SiMe_3)_2]$ as a size-control additive, and affords narrowly dispersed nanocrystals over the size range of 3−115 nm.[5] However, the synthesis was developed empirically, and the nanocrystal growth mechanism was not understood.

In the above procedure, the Bi-nanocrystal size distributions (CSDs) were observed to evolve in an interesting manner with time. An initial burst of small nanocrystals was followed by the emergence of distinctly larger nanocrystals interspersed among the smaller nanocrystals at early times. We have previously found such observations to be consistent with an aggregative nanoparticle growth mechanism.[26,27] Consequently, we have undertaken the detailed study reported here to confirm the growth mechanism, and to thereby determine if the synthetic results above can be extended or generalized.

Previous studies have demonstrated that aggregative growth may be nucleation driven,[26−28] and we have

*To whom correspondence should be addressed. E-mail: buhro@wustl.edu.

(1) Yu, H.; Gibbons, P. C.; Kelton, K. F.; Buhro, W. E. *J. Am. Chem. Soc.* **2001**, *123*, 9198–9199.
(2) Yu, H.; Li, J.; Loomis, R. A.; Gibbons, P. C.; Wang, L.-W.; Buhro, W. E. *J. Am. Chem. Soc.* **2003**, *125*, 16168–16169.
(3) Yu, H.; Gibbons, P. C.; Buhro, W. E. *J. Mater. Chem.* **2004**, *14*, 595–602.
(4) Wang, F.; Dong, A.; Sun, J.; Tang, R.; Yu, H.; Buhro, W. E. *Inorg. Chem.* **2006**, *45*, 7511–7521.
(5) Wang, F.; Tang, R.; Yu, H.; Gibbons, P. C.; Buhro, W. E. *Chem. Mater.* **2008**, *20*, 3656–3662.
(6) Grebinski, J. W.; Hull, K. L.; Zhang, J.; Kosel, T. H.; Kuno, M. *Chem. Mater.* **2004**, *16*, 5260–5272.
(7) Hull, K. L.; Grebinski, J. W.; Kosel, T. H.; Kuno, M. *Chem. Mater.* **2005**, *17*, 4416–4425.
(8) Fanfair, D. D.; Korgel, B. A. *Cryst. Growth Des.* **2005**, *5*, 1971–1976.
(9) Dong, A.; Wang, F.; Daulton, T. L.; Buhro, W. E. *Nano Lett.* **2006**, *7*, 1308–1313.
(10) Kuno, M.; Ahmad, O.; Protasenko, V.; Bacinello, D.; Kosel, T. H. *Chem. Mater.* **2006**, *18*, 5722–5732.
(11) Davidson, F. M.; Lee, D. C.; Fanfair, D. D.; Korgel, B. A. *J. Phys. Chem. C* **2007**, *111*, 2929–2935.
(12) Wang, F.; Yu, H.; Li, J.; Hang, Q.; Zemlyanov, D.; Gibbons, P. C.; Wang, L.-W.; Janes, D. B.; Buhro, W. E. *J. Am. Chem. Soc.* **2007**, *129*, 14327–14335.
(13) Fanfair, D. D.; Korgel, B. A. *Chem. Mater.* **2007**, *19*, 4943–4948.
(14) Dong, A.; Tang, R.; Buhro, W. E. *J. Am. Chem. Soc.* **2007**, *129*, 12254–12262.
(15) Wang, F.; Buhro, W. E. *J. Am. Chem. Soc.* **2007**, *129*, 14381–14387.
(16) Dong, A.; Yu, H.; Wang, F.; Buhro, W. E. *J. Am. Chem. Soc.* **2008**, *130*, 5954–5961.
(17) Sun, J.; Wang, L.-W.; Buhro, W. E. *J. Am. Chem. Soc.* **2008**, *130*, 7997–8005.
(18) Wang, F.; Tang, R.; Buhro, W. E. *Nano Lett.* **2008**, *8*, 3521–524.
(19) Puthussery, J.; Lan, A.; Kosel, T. H.; Kuno, M. *ACS Nano* **2008**, *2*, 357–367.
(20) Wang, F.; Yu, H.; Jeong, S.; Pietryga, J. M.; Hollingsworth, J. A.; Gibbons, P. C.; Buhro, W. E. *ACS Nano* **2008**, *2*, 1903–1913.
(21) Sun, J.; Buhro, W. E. *Angew. Chem., Int. Ed.* **2008**, *47*, 3215–3218.
(22) Fanfair, D. D.; Korgel, B. A. *Cryst. Growth Des.* **2008**, *8*, 3246–3252.
(23) Wang, F.; Tang, R.; Kao, J. L.-F.; Dingman, S. D.; Buhro, W. E. *J. Am. Chem. Soc.* **2009**, *131*, 4983–4996.
(24) Trentler, T. J.; Hickman, K. M.; Goel, S. C.; Viano, A. M.; Gibbons, P. C.; Buhro, W. E. *Science* **1995**, *270*, 1791–1794.
(25) Trentler, T. J.; Goel, S. C.; Hickman, K. M.; Viano, A. M.; Chiang, M. Y.; Beatty, A. M.; Gibbons, P. C.; Buhro, W. E. *J. Am. Chem. Soc.* **1997**, *119*, 2172–2181.
(26) Shields, S. P.; Richards, V. N.; Buhro, W. E. *Chem. Mater.* **2010**, *22*, 3212–3225.
(27) Richards, V. N.; Rath, N. P.; Buhro, W. E. *Chem. Mater.* **2010**, *22*, 3556–3567.

Published on Web 12/23/2010

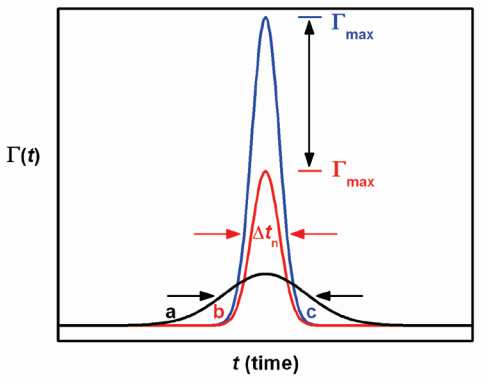

Figure 1. Three schematic nucleation functions a−c having Gaussian profiles. The 2σ width of the nucleation function (Δt_n) provides a measure of the time window for nucleation. Because the Δt_n for function b is smaller than that for function a, the nucleation process described by function b will produce a narrower nanoparticle size distribution. Functions b and c have identical Δt_n values. However, function c has a greater maximum nucleation rate Γ_{max} and thus a larger under-curve area, which is N, the number of nucleated nanoparticles. Thus, with an equal amount of precursor, the nucleation process described by function c will ultimately produce a smaller final nanoparticle mean size.

argued that aggregative nucleation provides a means for the purposeful manipulation of final nanoparticle mean sizes and size distributions. Nucleation typically occurs in an early time window that by necessity precedes growth.[29,30] In aggregative nucleation, the process corresponds to the assembly of a critical-sized aggregate of small, primary nanocrystals, which may subsequently coalesce to a single-crystalline or polycrystalline nanoparticle that is viable for further aggregative growth.

Schematic diagrams of nucleation functions, which describe the time dependence of the nucleation rate $\Gamma(t)$, are given in Figure 1. The (2σ) width of the nucleation function Δt_n determines the width of the final nanoparticle size distribution. To obtain a narrow size distribution, conditions that minimize Δt_n must be identified. The area under the nucleation function is N, the number of nuclei formed, which is the number of growing nanoparticles. The amount of precursor used and N determine the final nanoparticle mean size. Ideally, N would be controlled by systematic changes in the maximum nucleation rate Γ_{max}, while maintaining a minimized Δt_n.

In a previous study of the coarsening of Au nanocrystals,[26] we demonstrated that Δt_n and N were systematically influenced by the concentration of a salt additive, tetraoctylammonium bromide. We further showed that the final Au-nanoparticle size and size distribution were strongly correlated with Δt_n and N in the manner described above. However, prior to the present results, we had not found experimental conditions that systematically influenced Γ_{max}. Thus, the aggregative growth of Bi nanocrystals provides an opportunity to further test the nucleation-control strategy described above and depicted in Figure 1.

(28) Prakash, A.; Bapat, A. P.; Zachariah, M. R. *Aerosol Sci. Technol.* **2003**, *37*, 892–898.
(29) LaMer, V. K.; Dinegar, R. H. *J. Am. Chem. Soc.* **1950**, *72*, 4847–4854.
(30) LaMer, V. K. *Ind. Eng. Chem.* **1952**, *44*, 1270–1277.

Here we report the kinetics of Bi-nanoparticle growth from $Bi[N(SiMe_3)_2]_3$ in the presence of varying concentrations of the additive $Na[N(SiMe_3)_2]$. We find that the additive concentration primarily influences Γ_{max}, whereas Δt_n remains reasonably narrow. We show that the nanoparticle mean size correlates strongly with Γ_{max}, and the nanoparticle size distribution correlates strongly with Δt_n, as expected, prior to the onset of Ostwald ripening. The results establish that important advances in nanoparticle synthesis by aggregative nucleation and growth will be realized when Γ_{max} and Δt_n can be purposefully, systematically controlled. A table of abbreviations used is provided as Supporting Information (Table S1).

Experimental Section

General Methods and Materials. Poly(1-hexadecene-*co*-1-vinylpyrrolidinone) (PHD-*co*-PVP, CAS No. 63231−81−2, also known as poly(1-vinylpyrrolidone)-graft-(1-hexadecene)) was used as received from Aldrich. This polymer is no longer available from the Aldrich catalog, but can be obtained as Ganex V-216 (PHD-*co*-PVP, CAS No. 63231−81−2) from ISP Technologies Inc. (contact: Ruthann Mekita (RMekita@ispcorp.com), 1361 Alps Rd, Wayne, NJ 07470). The PHD-*co*-PVP provided by Aldrich had an average M_n of 2,500 Da, an M_p (peak molecular weight) of 2800 Da, and a polydispersity index (PDI) of 1.9. $Na[N(SiMe_3)_2]$ (as a 1.0 M THF solution packaged under N_2), toluene, and methanol were purchased from Aldrich and used as received. 1,3-diisopropylbenzene (DIPB) was purchased from Aldrich, shaken with concentrated sulphuric acid to remove thiophene, neutralized with K_2CO_3, washed with water, and distilled over Na. The precursor $Bi[N(SiMe_3)_2]_3$ was synthesized according to the literature[4] and stored in the freezer in the glovebox. A solution containing 25% w/w PHD-*co*-PVP in diisopropylbenzene (DIPB) was prepared using dry DIPB and stored in the glovebox over molecular sieves. All kinetics trials were conducted in a dry O_2-free N_2 atmosphere using standard air-free techniques under ambient pressure. The purification of the Bi nanocrystals taken from aliquots during the kinetics trials was conducted in the ambient atmosphere, as was TEM sample preparation.

Collection of Kinetic Data for Bismuth Nanoparticle Growth. $Bi[N(SiMe_3)_2]_3$, (69 mg, 0.10 mmol) was dissolved in the 25 wt % PHD-*co*-PVP in DIPB (10 g) in a Schlenk tube, generating a pale yellow solution. To this solution was added $Na[N(SiMe_3)_2]$ (450 mg, 0.498 mmol). The mixture was then placed in a 2.6 L oil bath that had been preheated to 180.0 ± 0.1 °C under the control of an Ace Glass temperature controller. Constant temperature was maintained and monitored with a Pt thermocouple. As the sample was heated, a light brown color developed within 5 min, which then gradually changed to a deep brown-black color within 10−20 min.

Removal of aliquots at prescribed times was performed by taking up a small volume of solution (0.3−0.5 mL) using a syringe needle and a new disposable syringe. Each aliquot was immediately redispersed into a test tube containing 0.5 mL of toluene. Methanol (4 mL) was immediately added to precipitate the nanocrystals. The methanol mixture containing the nanoparticles was then centrifuged for 2 min. After centrifuging, the methanol was removed. The toluene-methanol-centrifugation process was then repeated.

After purification, 0.5 mL toluene was added to the isolated nanocrystals and the mixture was sonicated for about 1 min. TEM grids were prepared within 1 h by the method described in

Table 1. Aggregative Nucleation, Growth and Ostwald Ripening Parameters Extracted from the Kinetic Data for Bi-Nanoparticle Growth As a Function $Na[N(SiMe_3)_2]$ Concentration

$Na[N(SiMe_3)_2]$ (M) (Na:Bi mole ratio)	τ_n (min)[a]	Δt_n (min)[b]	k_g ($\times 10^{-2}$ s^{-1})[c]	n[d]	τ_{OR} (min)[e]	k_{OR} ($\times 10^{-3}$ s^{-1})[f]	d_{final} (nm)	N ($\times 10^{14}$)[g]	Γ_{max} ($\times 10^{11}$ s^{-1})[h]
0.049 (4.90:1)	38.33 ± 0.89	26.69 ± 1.51	1.37 ± 0.02	3.04 ± 0.18	117.71 ± 10.21	2.48 ± 0.22	29.13 ± 0.32	2.60 ± 0.19	1.29 ± 0.08
0.063 (6.30:1)	41.42 ± 0.79	21.41 ± 1.60	1.51 ± 0.02	3.57 ± 0.28	78.95 ± 4.69	8.10 ± 0.74	20.86 ± 0.19	7.19 ± 0.85	4.47 ± 0.04
0.076 (7.60:1)	38.25 ± 1.10	19.71 ± 1.55	1.68 ± 0.06	3.76 ± 0.69	75.56 ± 7.86	6.28 ± 0.55	20.11 ± 0.09	9.17 ± 0.70	6.19 ± 0.02
0.087 (8.70:1)	36.07 ± 0.73	18.27 ± 0.97	1.62 ± 0.02	4.36 ± 0.38	88.32 ± 8.68	3.88 ± 0.38	23.15 ± 0.09	5.42 ± 0.33	3.95 ± 0.02
0.099 (9.99:1)	47.36 ± 0.85	28.83 ± 1.56	1.15 ± 0.03	3.89 ± 0.47	105.04 ± 14.65	3.47 ± 0.42	24.48 ± 0.19	4.30 ± 0.22	2.03 ± 0.02

[a] Time taken for maximum nucleation rate to be achieved. [b] Time window for nucleation. [c] Growth rate. [d] Avrami exponent. [e] Onset time for Ostwald ripening. [f] Rate parameter for Ostwald ripening. [g] Total number of critical aggregates. [h] Maximum nucleation rate.

the next section. In subsequent kinetics trials, all conditions were held constant except the amount of $Na[N(SiMe_3)_2]$, which was varied as follows; 569 mg (0.631 mmol), 690 mg (0.764 mmol), 785 mg (0.869 mmol) and 903 mg (0.999 mmol). Nanoparticles purified very quickly after the aliquot was taken gave the cleanest TEM images.

Measurement of Nanocrystal Size and Size Distribution. Carbon Type-B, 300-mesh copper grids (Ted Pella) were used with the carbon support intact. The toluene solution of nanoparticles was further diluted as necessary to ensure a light coverage. One to two drops of the solution were pipetted onto the grid in air and tapped lightly to remove the excess. The prepared sample was then evaporated to dryness, taking care to protect it from heat exposure, as this could cause agglomeration and ripening. All samples were prepared within 1 h of sample purification, and were analyzed by TEM within 24 h of grid preparation. No evidence of particle agglomeration was observed during TEM analysis. Digital TEM images were obtained from several locations on the sample grid using a JEOL 2000 FX instrument operating at 200 kV. The normal bright-field images were saved in a TIF format and resampled using Corel PHOTO-PAINT 9 (www.corel.com), increasing the resolution from 72 to 400 dpi. The particle diameter distributions were measured from multiple images using Image-Pro Express software (www.mediacy.com). A minimum of 400 particles were measured for each sample, and all particles in a given image were measured to obtain the most accurate ratio of small to large particles, as this greatly affected the average diameter obtained. The number of particles measured was particularly important for the bimodal early time distributions, as these samples required larger numbers of particles to form an accurate distribution. Periodically, 2000 or more particles were measured in order to compare the mean, standard deviation, and distribution shape to those obtained from smaller sample counts. No significant difference was detected on these occasions, indicating that the number of particles measured was sufficient to produce reliable statistics.

Analysis of Kinetics Data. The diameter distributions obtained from TEM images at each time point were converted to volume distributions by assuming spherical morphologies. At each time point, the fraction of nanoparticles in the distribution having the critical size (F_{crit}) was determined by dividing the number of nanocrystals in the critical-size bin by the total number of nanoparticles counted. As described in the Results section, two critical bin sizes were investigated, corresponding to critical diameters of 3.0−3.5 and 3.5−4.0 nm.

The nucleation functions F_{crit} vs time were plotted for each kinetics trial and fit with Gaussians using Origin software (www.OriginLab.com). The maximum aggregative nucleation rate Γ_{max} (Table 1) was determined and the nucleation functions scaled as $\Gamma(t)$ by the following procedure. The total number N (Table 1) of aggregative nuclei formed was calculated by dividing the total volume of Bi used by the final mean nanocrystal volume at the conclusion of aggregative growth ($\overline{V}_{lim}$). Γ_{max}, the height of the fitted Gaussian, was then calculated from $N/[\Delta t_n(\pi/2)^{1/2}]$, where Δt_n (Table 1) is the 2σ width of the Gaussian.[26] Finally, the y axes of the nucleation functions were rescaled as $\Gamma(t)$ (converting from F_{crit}) using the calculated values of Γ_{max}.

The kinetics data for each trial were then plotted as $\overline{V}(t)/\overline{V}_{lim}$ vs time, where $\overline{V}(t)$ is the mean nanocrystal volume determined from the volume distribution at each time point. The data for each trial were then fit to eq 1 using Origin software. The fitting parameters were k_g, n, k_{OR}, and τ_{OR}. The w parameter was arbitrarily assigned a value of 3 min, and was not optimized by fitting. These parameters are defined in the Results section, and their fitted values recorded in Table 1.

Results

Early Time Monitoring of Nanoparticle Growth. Bismuth nanoparticles were generated at 180 ± 0.1 °C by an adaptation of the previously reported method,[5] which was the thermolysis of mixtures of $Bi[N(SiMe_3)_2]_3$ and $Na[N(SiMe_3)_2]$ in the presence of the polymeric nanoparticle stabilizer PHD-*co*-PVP. The process was monitored by TEM. The earliest images at 2 min revealed large populations of small (hereafter identified as "primary") nanocrystals having a mean diameter of 1.9 ± 0.35 (one σ) nm (Figure 2a). At early times, a small population of significantly larger nanocrystals was interspersed among the primary nanocrystals (Figure 2a-d), producing bimodal size distributions. Such distributions are primary evidence of aggregative nucleation-and-growth mechanisms.[26,27,31−37] Over time, the nanocrystals in the larger mode grew, as the population of primary nanocrystals progressively diminished. In the Figure 2 trial, the primary nanocrystals had disappeared by 100 min (Figure 2e). Subsequently, broadened size distributions were observed (Figure 2f), indicative of Ostwald ripening.[27,38−41]

(31) Matijević, E.; Goia, D. *Croatica Chem. Acta* **2007**, *80*, 485–491.
(32) Privman, V.; Goia, D. V.; Park, J.; Matijević, E. *J. Colloid Interface Sci.* **1999**, *213*, 36–45.
(33) Libert, S.; Gorshkov, V.; Goia, D.; Matijević, E.; Privman, V. *Langmuir* **2003**, *19*, 10679–10683.
(34) Privman, V. *Ann. N.Y. Acad. Sci.* **2009**, *1161*, 508–525.
(35) Drews, T. O.; Katsoulakis, M. A.; Tsapatsis, M. *J. Phys. Chem. B* **2005**, *109*, 23879–23887.
(36) Drews, T. O.; Tsapatsis, M. *Microporous Mesoporous Mater.* **2007**, *101*, 97–107.
(37) Bogush, G. H.; Zukoski, C. F. *J. Colloid Interface Sci.* **1991**, *142*, 19–34.
(38) Talapin, D. V.; Rogach, A. L.; Haase, M.; Weller, H. *J. Phys. Chem. B.* **2001**, *105*, 12278–12285.

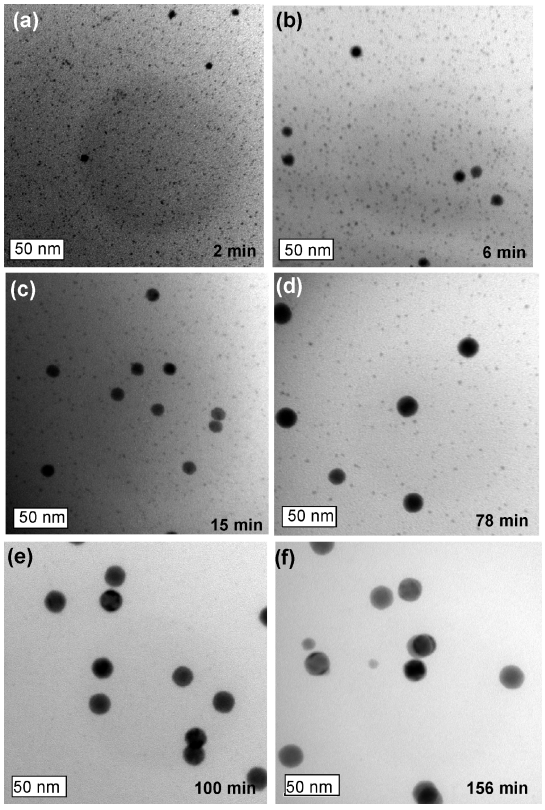

Figure 2. TEM images of aliquots taken at various times from a kinetics trial conducted at a $Na[N(SiMe_3)_2]$ concentration of 0.062 M. Bimodal size distributions are evident in a−d. The broadened distribution in f is due to Ostwald ripening.

Aggregative-Nucleation Functions. The bimodality evident in Figure 2a-d results from the formation of critical aggregates of primary particles (aggregative nuclei), which coalesce to nanoparticles that are viable for further aggregative growth.[26,27] We showed previously that the critical-aggregate size (expressed as a particle volume) is determined in favorable cases by the emergence of a peak in the early time CSDs. We also showed that the aggregative-nucleation function−the time dependence of the aggregative-nucleation rate−could be obtained from a plot of the fraction of nanoparticles having the critical size (F_{crit}) vs time.[26,27]

In the present study, peaks in the CSDs at the critical-aggregate sizes were not well resolved, because of the large diameter range over which growth occurred (1.9−29 nm). We were unable to count sufficiently large numbers of nanoparticles to provide highly resolved CSDs over the large nanoparticle-volume ranges observed (see Figure S1 in the Supporting Information). Consequently, we chose a critical-diameter bin size of 3.5−4.0 nm by correspondence to those found in our previous studies. We did so with the confidence that if we used a bin *smaller* than the true critical-aggregate size, a nucleation function could not be successfully extracted from the data. Furthermore, if we used a bin larger than the true critical-aggregate size, the nucleation function should be only slightly broadened (in Δt_n) and delayed relative to that obtained at the true size.

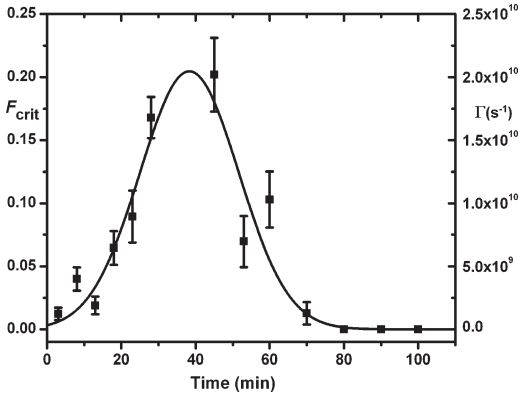

Figure 3. Nucleation function and Gaussian fit for a kinetics trial conducted at a $Na[N(SiMe_3)_2]$ concentration of 0.049 M. The left and right axes correspond to the critical-aggregate fraction F_{crit} and the scaled nucleation rate $\Gamma(t)$, respectively (see text).

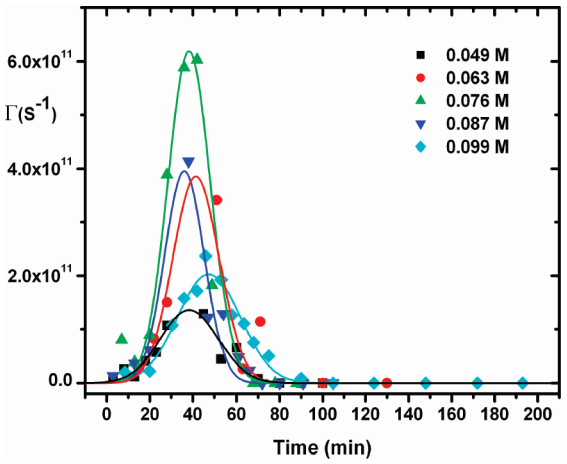

Figure 4. Nucleation functions for kinetics trials conducted at various $Na[N(SiMe_3)_2]$ concentrations. The individual $Na[N(SiMe_3)_2]$ concentrations are given in the inset legend.

A set of nucleation functions like those in Figures 1, 3, and 4 were constructed using the procedures we previously reported[26,27] and assuming a critical-diameter bin of 3.5−4.0 nm. We then redetermined the nucleation functions by assuming a critical-diameter bin of 3.0−3.5 nm. The two sets of functions were similar to one another, except that those determined at the smaller assumed critical size were shifted earlier in time, as expected, and gave less scatter in the F_{crit} data with respect to the Gaussian fits. These nucleation functions are given in Figures 3 and 4, and the quantitative values extracted from them were used in the remainder of this study.

As noted above, we previously found that $Na[N(SiMe_3)_2]$ functioned as a size-control additive in Bi-nanoparticle growth, and we hypothesized that it influenced the nucleation process.[5] Figure 3 is the F_{crit} vs t curve extracted from a kinetics trial using a $Na[N(SiMe_3)_2]$ concentration of 0.049 M. The curve was rescaled as the nucleation function $\Gamma(t)$ vs t (right axis in Figure 3) as previously described.[26,27]

(39) Sagui, C.; O'Gorman, D. S.; Grant, M. *Phys. Rev. E.* **1997**, *56*, R21–R24.
(40) Mantzaris, N. V. *Chem. Eng. Sci.* **2005**, *60*, 4749–4770.
(41) Chen, Y.; Johnson, E.; Peng, X. *J. Am. Chem. Soc.* **2007**, *129*, 10937–110947.

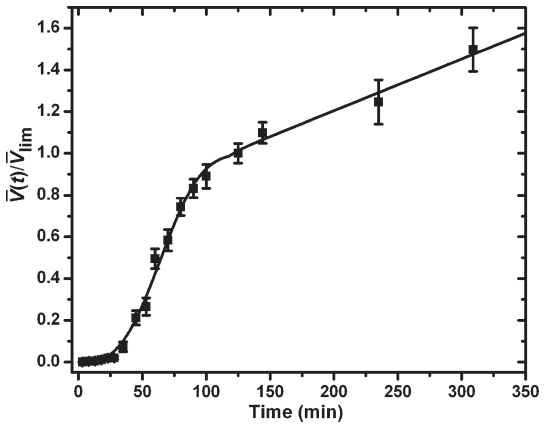

Figure 5. Kinetic data and the eq 1 fit for a kinetic trial conducted with a $Na[N(SiMe_3)_2]$ concentration of 0.049 M. $\overline{V}(t)$ is the nanocrystal mean volume at time t, and $\overline{V}_{lim}$ is the final nanocrystal mean volume (as defined in the text).

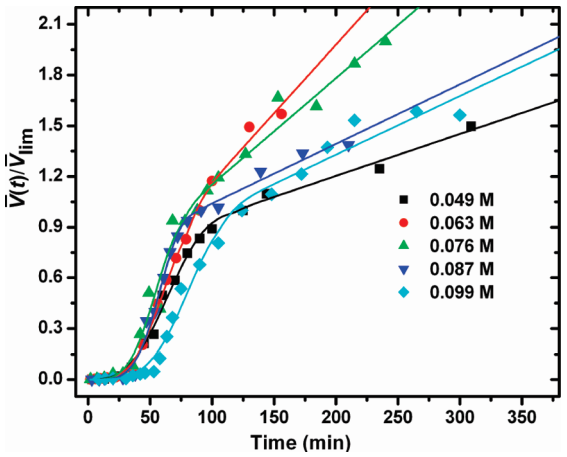

Figure 6. Kinetic data and the eq 1 fits for kinetics trials conducted at various $Na[N(SiMe_3)_2]$ concentrations. The individual $Na[N(SiMe_3)_2]$ concentrations are given in the inset legend.

Figure 4 gives the nucleation functions determined at all the $Na[N(SiMe_3)_2]$ concentrations studied. (Individual nucleation functions are plotted with error bars as Figures S2−S5 in the Supporting Information.) The maximum nucleation rate Γ_{max}, the time at which Γ_{max} was reached τ_n, and the (2σ) width of the time window for nucleation Δt_n taken from the Figure-4 nucleation functions are recorded in Table 1. The results reveal comparatively small differences in τ_n and Δt_n at the various $Na[N(SiMe_3)_2]$ concentrations, but significant variations in Γ_{max} (Figure 4 and Table 1). The implications of these nucleation-parameter comparisons are further developed in the Discussion. Clearly, the $Na[N(SiMe_3)_2]$ additive did indeed influence the aggregative-nucleation process.

Particle-Growth Kinetics. A representative kinetic profile for Bi-nanocrystal growth (obtained using a $Na[N(SiMe_3)_2]$ concentration of 0.049 M) is shown in Figure 5. The growth is plotted as $\overline{V}(t)/\overline{V}_{lim}$ vs time, where $\overline{V}(t)$ is the mean nanocrystal volume at time t, and $\overline{V}_{lim}$is the limiting mean nanocrystal volume at the end of the active-growth period (see below). $1/\overline{V}_{lim}$ is a scaling factor that allows kinetics fits from the different trials to be conveniently compared.

We have shown previously that pseudosigmoidal nanoparticle growth profiles may be well fit by eq 1.[27] The first term in eq 1 is a conventional KJMA expression to fit the aggregative nucleation and growth regimes.[26,42] The second term accounts for the late-time Ostwald ripening, during which the mean nanocrystal volume increases linearly with time.[27,43−46] This second, Ostwald-ripening term contains a logistic turn-on function that activates Ostwald ripening at an onset time τ_{OR}. The w parameter in eq 1 determines the width of the Ostwald-ripening turn-on period, which was arbitrarily set at 3 min. The parameters k_g and k_{OR} are rate parameters describing aggregative growth and Ostwald ripening, respectively, and n is the Avrami exponent. Nonlinear least-squares fitting by optimization of k_g, n, k_{OR}, and τ_{OR} in eq 1 afforded the fitted curve in Figure 5. The initial induction period is associated with aggregative nucleation, the steeply rising intermediate regime with aggregative growth, and the final slope with Ostwald ripening.

$$\frac{\overline{V}(t)}{\overline{V}_{lim}} = (1-\exp(-k_g t)^n) + \left[\frac{(t-\tau_{OR})}{1+\exp(-2w(t-\tau_{OR}))}\right]k_{OR} \quad (1)$$

All sets of kinetic data collected as a function of $Na[N(SiMe_3)_2]$ concentration are plotted in Figure 6, with their eq-1 fits. The individual plots with error bars are Figures S6−S9 in the Supporting Information. The fitted k_g, n, k_{OR}, and τ_{OR} values are recorded in Table 1. These values are analyzed in the Discussion. The curves exhibit quite similar pseudosigmoidal profiles, although a systematic variation in the Ostwald-ripening rate k_{OR} is clearly evident.

Discussion

Elucidating the Nucleation and Growth Pathway. As discussed previously, nanoparticles grown from molecular precursors are typically assumed to result from classical (LaMer) nucleation and growth, and nanoparticles grown from smaller nanoparticles are typically assumed to result from Ostwald ripening.[27] However, neither the classical mechanism nor Ostwald ripening can produce the bimodal size distributions in Figure 2a−d.[26] The observation of an initial burst of primary nanocrystals followed by the emergence of bimodal distributions containing distinctly larger nanoparticles is a strong indicator of aggregative processes.[26,27,31−37] Our recent study of Ag nanoparticle growth showed that all three mechanisms−classical nucleation growth, aggregative nucleation and growth, and Ostwald ripening−can participate, but can do so in largely consecutive time regimes with little overlap.[27] Indeed, the results contained in Figures 2−6

(42) Skrdla, P. J.; Robertson, R. T. *Chem. Mater.* **2008**, *20*, 3–4.
(43) Voorhees, P. W. *J. Stat. Phys.* **1985**, *38*, 231.
(44) Lifshitz, I. M.; Slyozov, V. V. *J. Phys. Chem. Solids.* **1961**, *19*, 35–50.
(45) Chen, M. K.; Voorhees, P. W. *Modell. Simul. Mater. Sci. Eng.* **1993**, *1*, 591–612.
(46) Vorhees, P. W. *Annu. Rev. Mater. Sci.* **1992**, *22*, 197–215.

establish the same overall pathway here: early-time classical nucleation and growth affording the primary nanocrystals, followed by aggregative nucleation and growth, followed by late-time Ostwald ripening.

Another key indicator of aggregative growth is the observation of polycrystalline mature nanoparticles.[26,27] Unfortunately, the very low bulk melting point of Bi (271 °C) leads to high atomic mobility at the growth temperature (180 °C), resulting in rapid recrystallization to single-crystalline nanoparticles.[5] Consequently, nanoparticle polycrystallinity or the lack of it are not useful here for distinguishing aggregative growth.

Nucleation Function and Nanocrystal Size and Size Distribution. The largest influences of $Na[N(SiMe_3)_2]$ concentration on the Bi-nanocrystal nucleation and growth kinetics are found in the maximum nucleation rate Γ_{max} and the Ostwald-ripening rate k_{OR} (see Table 1). The parameter Γ_{max} rises and falls with increasing $Na[N(SiMe_3)_2]$ concentration over a range in which the minimum and maximum values vary over a range of nearly 6 fold. The parameter k_{OR} rises and falls with increasing $Na[N(SiMe_3)_2]$ concentration over a range in which the minimum and maximum values vary over a range of nearly 4 fold. By contrast, the remaining kinetic parameters τ_n, Δt_n, k_g, and τ_{OR} vary over ranges that are within factors of less than 2. Thus, the added $Na[N(SiMe_3)_2]$ operates as both a nucleation-control and an Ostwald-ripening agent.

We argued above (Figure 1) and previously demonstrated[26] that the "final" nanoparticle size distribution should correlate with Δt_n, the time window for nucleation, and that the "final" nanoparticle mean size (d_{final}) should anticorrelate with N, the number of growing nanoparticles (and the area under the nucleation function described by Δt_n and Γ_{max}). Here the "final" size and size distribution refer to those just prior to the onset of Ostwald ripening at τ_{OR}. Because Δt_n was observed to vary over such a small range here, N is largely dependent on the variations in Γ_{max}. Consequently, we next examine the correlations between final size distribution and final mean size with Δt_n and Γ_{max}, respectively, as a function of $Na[N(SiMe_3)_2]$ concentration.

Figure 7 plots the relative standard deviation in the final nanocrystal size distribution and Δt_n vs $Na[N(SiMe_3)_2]$ concentration. The two curves follow one another fairly closely, indicating that the narrower nucleation time windows produce narrower final size distributions, as expected (see Figure 1). These results parallel those we previously reported for the coarsening of Au nanoparticles.[26]

Figure 8 plots the final nanocrystal mean diameter d_{final} and Γ_{max} vs $Na[N(SiMe_3)_2]$ concentration. The two curves are nearly mirror images of one another, showing that, at a fixed amount of Bi, a larger Γ_{max} and thus a larger N produce a smaller final mean nanocrystal size, as expected (see Figure 1). The values of d_{final} and Γ_{max} are indeed anticorrelated. These results are also consistent with those we previously reported for the coarsening of Au nanoparticles.[26]

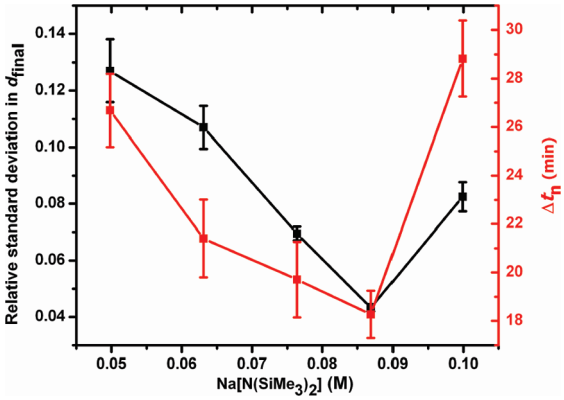

Figure 7. Plots of the relative standard deviation in the final nanocrystal diameter distribution (black squares, left axis) and the time window for nucleation Δt_n (red squares, right axis) as functions of $Na[N(SiMe_3)_2]$ concentration. The relative standard deviation is the standard deviation in the diameter at the end of the active growth regime divided by the final mean nanocrystal diameter.

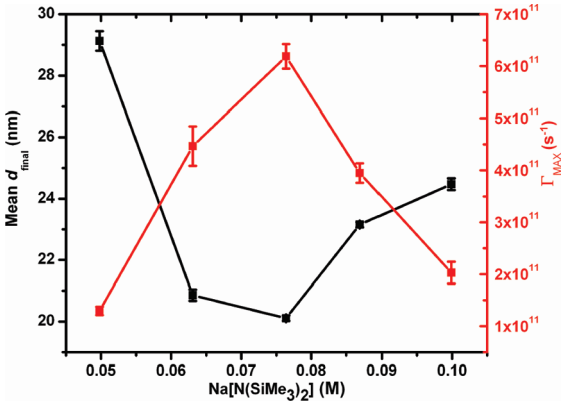

Figure 8. Plots of the final nanocrystal mean diameter (black squares, left axis) and the maximum nucleation rate Γ_{max} (red squares, right axis) as functions of $Na[N(SiMe_3)_2]$ concentration.

The rise and then fall in Γ_{max} with increasing $Na[N(SiMe_3)_2]$ concentration indicates that at lower concentrations the additive functions as a nucleation promoter, and at higher concentrations as a nucleation inhibitor. In our prior study, we argued that an ionic additive promoted aggregative nucleation by collapsing the electric double layer around the nanoparticles that stabilized them against aggregation (Scheme 1).[47] This affect presumably accounts for the influence of $Na[N(SiMe_3)_2]$ at lower concentrations. At higher concentrations, the additive apparently performs a second, presently unidentified function that inhibits aggregative nucleation. A speculative possibility is that attachment of additional $N(SiMe_3)_2$ ligands to the nanocrystal surfaces increases the steric barrier to aggregation (Scheme 1).

Potential support for the latter speculation may be drawn from comparisons of the aggregative-nucleation kinetics for Bi nanocrystals in this study, and for Au[26] and Ag[27] nanoparticles from our previous studies. As shown in Table 2, the maximum nucleation rate is 2 orders of magnitude lower for Bi. The number of aggregative nuclei

(47) Hiemenz, P. C.; Rajagopalan, R. *Principles of Colloid and Surface Chemistry*, 3rd ed.; Marcel Dekker: New York, 1997; pp 585−604.

Scheme 1. Schematic Depiction of the Speculative Roles of $Na[N(SiMe_3)_2]$ in the Promotion and Inhibition of Aggregative Nucleation[a]

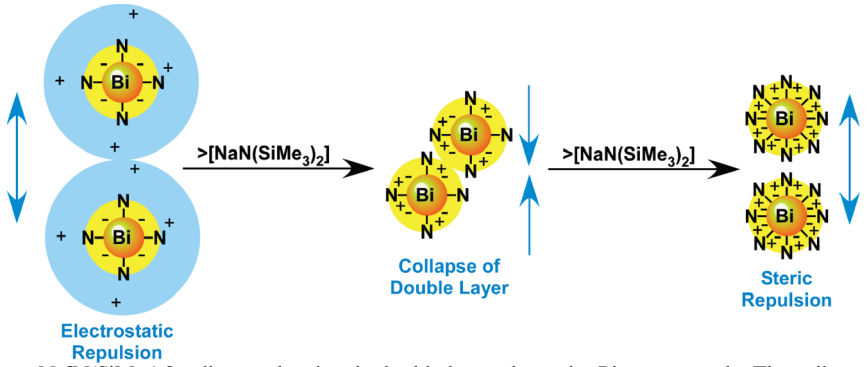

[a] At lower concentrations, $Na[N(SiMe_3)_2]$ collapses the electric double layer about the Bi nanocrystals. The yellow region surrounding the Bi nanocrystal core represents the polymer coating, and the light-blue region represents the double-layer (the extent of the Na^+counterion atmosphere). The Na^+ ions are depicted by plus signs, and the $[N(SiMe_3)_2]^-$ ligands attached to the Bi surfaces by minus signs and N symbols. At low ionic strength (left) the Na^+ counterion atmosphere is extended due to mutual Na^+ ion repulsions. The extended Na^+ counterion atmospheres on adjacent nanoparticles repel one another, preventing the close approach of nanoparticles, and thus inhibiting their aggregation. At higher ionic strength (center) the double layer collapses because of screening, and the counterion atmosphere about each nanoparticle shrinks dramatically, promoting the aggregation of nanoparticles. At even higher concentrations, additional $[N(SiMe_3)_2]^-$ ligands attach to the Bi-nanocrystal surfaces, increasing the steric barrier (right) and inhibiting aggregation.

Table 2. Maximum Nucleation Rate and the Number of Aggregative Nuclei Formed Per Mole of Metal for the Aggregative Growth of Au, Ag, and Bi Nanocrystals

nanocrystals	Γ_{max} (s^{-1})	N/mol (nuclei mol^{-1})
Au[a]	2.63×10^{13}	6.99×10^{19}
Ag[a]	1.21×10^{13}	5.04×10^{19}
Bi	6.19×10^{11}	9.17×10^{18}

[a] The data were taken from refs 26 and 27 for Au and Ag, respectively.

formed per mole of metal is 1 order of magnitude lower for Bi, establishing a larger comparative aggregative-nucleation barrier. The smaller nucleation rates and numbers for Bi account for the larger final mean diameters of the Bi nanoparticles (20−29 nm) compared to those of Au (5−7 nm) and Ag (7−8 nm).

In the case of Ag, there was presumably no electrostatic component to the aggregative-nucleation barrier.[27] For Au, the electrostatic barrier resulted from surface-adsorbed bromide ions, which are sterically small.[26] For Bi, the putative electrostatic barrier results from surface-adsorbed $[N(SiMe_3)_2]^-$ ligands, which are very bulky. Consequently, one should expect a larger steric component to the aggregative-nucleation barrier for Bi, both before and after collapse of the electrostatic component (Scheme 1).

Ostwald Ripening. As noted above, $Na[N(SiMe_3)_2]$ also behaves as an Ostwald-ripening agent under the conditions employed here, as evidenced by the increase and then decrease in the Ostwald-ripening rate k_{OR} with increasing $Na[N(SiMe_3)_2]$ concentration. Ostwald-ripening agents generally function by altering the concentrations or populations of the mobile transport species involved in the exchange of material between smaller and larger particles.[48−52] In the present case $Na[N(SiMe_3)_2]$ is presumably involved in the generation of soluble Bi complexes that participate in Bi transport.

Ostwald-ripening agents are known to influence nucleation under certain conditions, as we have observed here.[48] Thus, an additive in amounts above a critical concentration can readily function as both a nucleation-control agent and an Ostwald-ripening agent. For synthetic purposes, one would ideally identify conditions under which the additive influences nucleation, in this case aggregative nucleation, but does not activate Ostwald ripening such that k_{OR} remains very small.

Fortunately, under the synthetic conditions we previously reported,[5] the rates of Ostwald ripening were vanishingly small. Those conditions employed higher $Bi[N(SiMe_3)_2]_3$ concentrations and lower $Na[N(SiMe_3)_2]$:$Bi[N(SiMe_3)_2]_3$ ratios than were studied here. Thus, apart from presence of Ostwald ripening, the mechanism elucidated in this study applies to the synthetic conditions, and establishes that size control resulted from systematic variations in Γ_{max} achieved by varying the $Na[N(SiMe_3)_2]$ concentration.

Conclusion

We proposed above (and in Figure 1) that ideal nucleation control over nanocrystal formation requires a narrow time window for nucleation Δt_n to ensure a narrow final size distribution, and an adjustable maximum nucleation rate Γ_{max} to allow systematic variation of the final mean size. In the present work, we have indeed achieved a systematic variation in Γ_{max} while maintaining a small Δt_n by addition of the nucleation-control agent $Na[N(SiMe_3)_2]$. The final Bi-nanocrystal size distributions and mean sizes have been shown to vary in the predicted manner.

The results establish that the proposed, ideal form of nucleation control has been achieved, although only in a limited sense. We do not understand precisely how the nucleation-control agent influences Γ_{max}, nor why it has such a small effect on Δt_n. Paradoxically, in our previous

(48) Leubner, I. H. *J. Imaging Sci.* **1987**, *31*, 145–148.
(49) Iwasaki, M.; Tanoue, H.; Satsu, K.; Tanaka, T. *J. Imaging Sci. Technol.* **1995**, *39*, 402–406.
(50) Lai, X.; Goodman, W. *J. Mol. Catal. A* **2008**, *162*, 33–50.
(51) Ott, L. S.; Finke, R. G. *Chem. Mater.* **2008**, *20*, 2592–2601.
(52) Layson, A. R.; Evans, J. W.; Thiel, P. A. *Phys. Rev. B.* **2002**, *65*, 193409.

study of Au-nanoparticle growth[26] the nucleation-control agent (tetra-*n*-octylammonium bromide) exerted a strong influence on Δt_n, and little effect on Γ_{max}. Consequently, the next stage of this work will require that we determine the detailed mechanisms by which Δt_n and Γ_{max} may be separately, purposefully adjusted. Progress in that work should allow true rational control in nanoparticle synthesis to be realized.

Acknowledgment. We thank Dr. Fudong Wang (Washington University) for helpful discussions. We are grateful to the National Science Foundation for funding this work under Grant CHE-1012898.

Supporting Information Available: List of abbreviations, representative CSDs, all nucleation functions and fits, and all kinetic data and fits (PDF). This material is available free of charge via the Internet at http://pubs.acs.org.